Ion exchange in complexing media – Nickel removal from ammoniacal ammonium sulfate solutions

Laatikainen Markku, Sainio Tuomo

DOI: 10.1016/j.cej.2019.05.128

Contents lists available at ScienceDirect

Chemical Engineering Journal

journal homepage: www.elsevier.com

Ion exchange in complexing media – Nickel removal from ammoniacal ammonium sulfate solutions

Markku Laatikainen *, Tuomo Sainio

LUT University, School of Engineering Science, Separation and Purification Technology, Yliopistonkatu 34, 53850 Lappeenranta, Finland

ARTICLE INFO

Keywords:
Chelating ion exchange
Complexation
Nickel
Ammonium sulfate
Ammonia
Modeling

ABSTRACT

In real hydrometallurgical systems, ion exchange of metal cations is often accompanied by competing processes, such as complex formation. In this paper, we have analyzed influence of complex formation on nickel uptake in a chelating ion exchanger that contains iminodiacetate groups. Both outer-sphere complexation with sulfate and inner-sphere complexation with ammonia were studied at 22 and 80 °C. In ammoniacal ammonium sulfate matrix, both these complexes are formed and prediction of nickel uptake becomes challenging. According to the results, nickel uptake can be substantially enhanced by complex formation. Under acidic conditions and at 80 °C, proton is complexed by sulfate more effectively than nickel and as a result, the exchange equilibrium favors nickel uptake. High sulfate background concentration further enhances the positive effect. In ammonium sulfate solutions, however, complexation with ammonia is needed to prevent nickel precipitation. The solution is stable near pH 7 and high nickel uptake can be obtained, because competition by H^+ is practically absent and Ni^{2+}/NH_4^+ selectivity is high. Complexation with NH_3 thus makes the conditions favorable for Ni uptake rather than affects directly on Ni exchange. All these findings were successfully correlated with a dynamic model including pertinent complexation and dissociation equilibria.

List of symbols

c	molar concentration, mol/L
d_p	average particle diameter, m
D_p	pore diffusion coefficient, m^2/s
D_{ax}	axial dispersion coefficient, m^2/s
h	NICA parameter, –
k	rate constant, 1/s
K_a	dissociation constant, –
L_b	bed length, m
M	molar mass, g/mol
N	number of mixing stages, –
N_R	number of reactions, –
r	reaction rate, mol/(dm^3s)
t	time, s
T	temperature, °C
v	interstitial velocity, m/s
x	axial coordinate, m
z	charge number, –
β	stability constant,
ε_b	bed void fraction, –
ε_p	pore void fraction, –
κ	affinity constant,
ν	stoichiometric coefficient, –

Subscripts and superscripts

0	initial, pure component or infinite dilution value
eluent	value in eluent
feed	value in feed
i, j, k	component, reaction, mixing stage
p	pore solution
w	water

Abbreviations

BV	bed volume
TP 207	iminodiacetate resin

* Corresponding author.
Email address: markku.laatikainen@lut.fi (M. Laatikainen)

https://doi.org/10.1016/j.cej.2019.05.128
Received 11 March 2019; Received in revised form 30 April 2019; Accepted 20 May 2019
Available online xxx

Table 1
Properties of TP 207 in acid form.

Average particle size (D50), mm	0.55
Functional group	$-N(CH_2COOH)_2$
Permanent porosity[a], –	0.33
Density[b], kg/L	0.55
Bed capacity[c], equiv/L	2.24

[a] Estimated by the incipient wetness method.
[b] Polymer content in the swollen resin. Estimated from the water sorption data.
[c] Fully protonated, measured by frontal analysis.

Table 2
Composition of the feed solutions. Concentrations are in mol/L.

	Feed A	Feed B	Feed C	Feed D
$NiCl_2$	0.017	–	–	–
$NiSO_4$	–	0.017	0.017	0.017
Na_2SO_4	–	–	1.0	–
$(NH_4)_2SO_4$	–	–	–	3.4
pH	4.8	4.9	5.0	7.0–8.5

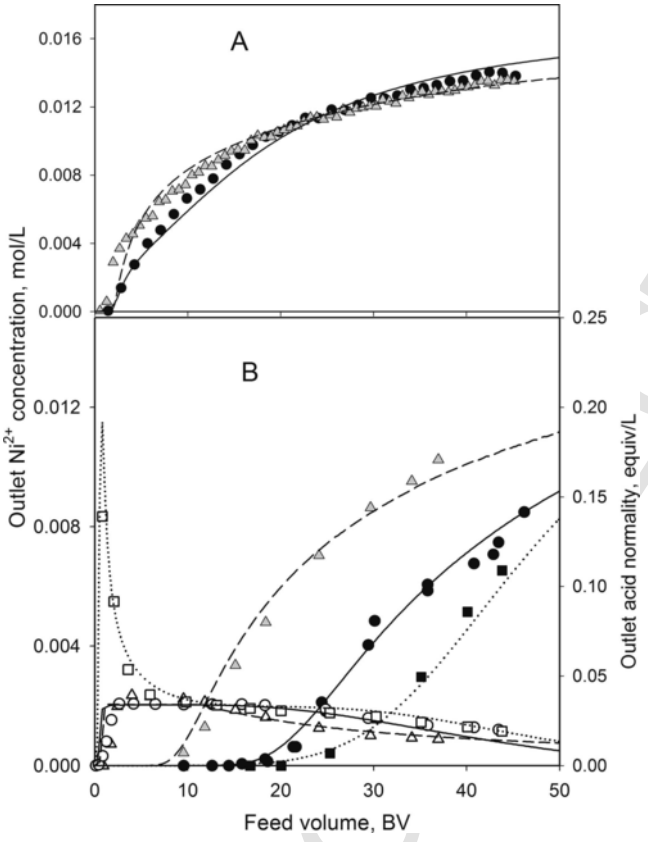

Fig. 1. Nickel (filled symbols) and acid (open symbols) outlet profiles in TP207 bed at 22 °C (A) and 80 °C (B). Feed solution: A (triangles), B (circles), C (squares). Feed rate was 2.8 BV/h at 22 °C and 8.3 BV/h at 80 °C.

1. Introduction

Ion exchange of heavy metals is a well-established technology in hydrometallurgical processing and in water treatment [1–3]. Cation exchangers carrying negatively charged functional groups are typically used to bind the hydrated metal cations from the solution phase [4]. Simple sulfonic acid or carboxylic acid resins have only moderate selectivity for the heavy metals and, therefore, chelating resins containing more advanced exchange sites are used. Iminodiacetate (*ida*) group, for example, binds transition metals by combined ion exchange and coordination mechanism leading to high selectivity even at moderately acidic conditions [5,6]. The selectivity gain is vital in cases, where small amounts of heavy metals are removed from a solution containing high concentrations of non-complexing cations.

Complexation of the target metal cations in the solution phase may affect the exchange process in different ways depending on the properties of the ligand. With neutral ligands like ammonia, the cation charge is retained but the selectivity may change depending on the degree of coordination [7,8]. Anionic ligands, on the other hand, neutralize or even reverse the charge thus rendering the cations inactive for cation exchange. Complexation is thus a competing process for ion exchange and as a result, metal uptake in the resin phase tends to decrease. Depending on the stability constants of the complexes in the bulk solution and in the resin, the effect may be negligible or ion exchange may become impossible.

Use of ion exchangers in complexation studies is well-established [9] but little attention has been paid on complexation in actual separation processes. In this paper we show that complexation in the bulk phase may in some cases be beneficial for the metal uptake. In particular, recovery of nickel from ammoniacal ammonium sulfate ($(NH_4)_2SO_4$-NH_3) solutions is considered, where complexation with both ammonia and sulfate anion takes place. Nickel *ammine* complexes are well-known examples of inner-sphere coordination, while outer-sphere complexation (or ion association) with sulfate is often considered unimportant and therefore overlooked. In hydrometallurgy, such complex solutions stem from oxidative leaching of nickel concentrates and subsequent nickel reduction processes [10]. In the reduction step, nickel is complexed with NH_3 and then reduced by H_2 at 110–120 °C to metallic Ni. The residual nickel concentration in the $(NH_4)_2SO_4$ solution is typically 1–2 g/L and pH is around 7. After removal of nickel and other heavy metals, the concentrated ammonium sulfate solution can be re-used or sold as fertilizer. Pajunen and Sheedy [11,12] have reported an ion-exchange process for such purposes and the feed solution was treated with the *ida* resin using the short-bed technology. In their case, cobalt removal was the main concern and nickel concentration in the feed was low.

The objective of this study is to investigate in detail the nickel uptake from synthetic ammoniacal ammonium sulfate solution containing 0.017 mol/L (1 g/L) of nickel and 3.4 mol/L (450 g/L) of ammonium sulfate. In particular, the role of complexation with sulfate anion and ammonia in nickel uptake was studied. Using a commercial *ida* resin in acid form, the metal uptake was measured in stirred-tank and fixed-bed systems. The measurements were made at ambient temperature and at 80 °C. The latter value was a compromise between the actual process temperature and resin thermal stability. The experimental data were correlated using an ion-exchange equilibrium model reported previously [13] and an approximate formulation of the Nernst-Planck diffusion model. These models were selected in order to properly account for the different exchange stoichiometry and the different diffusion rates of the uni- and di-valent cations. Complexation and dissociation reactions taking place in the bulk solution and resin pores were also accounted for. The purpose of extensive model calculations was to provide a physically relevant framework, where the contribution of individual processes can be evaluated on the basis of the experimental results. The selected model system is reasonably complicated but still well-defined and, moreover, it has practical importance in industrial hydrometallurgy.

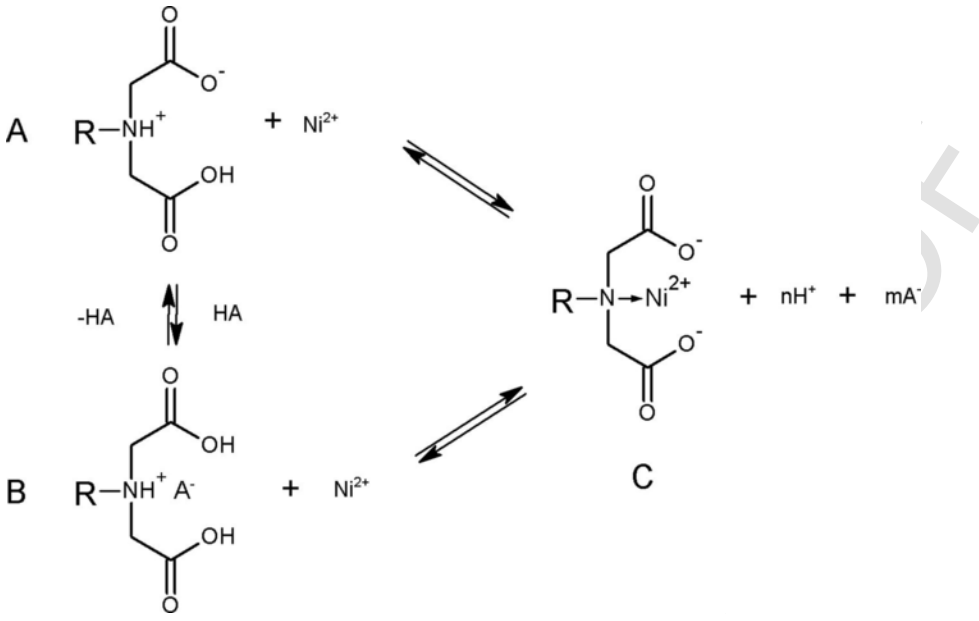

Fig. 2. H/Ni exchange in the diprotonated (A) and triprotonated (B) *ida* groups. R stands for the polymer matrix and A^- is a univalent anion.

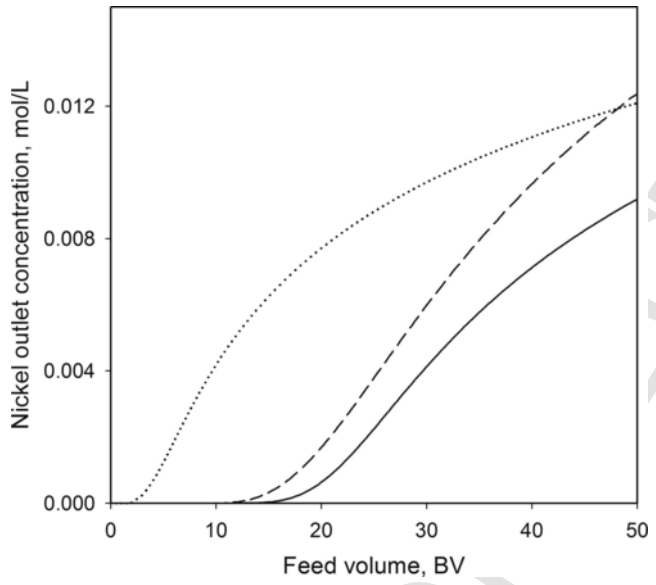

Fig. 3. Nickel breakthrough curves calculated with the model parameters of Table 3. Solid line: formation of HSO_4^- and $[NiSO_4]^0$ included; dashed line: no reactions included; dotted line: only formation of $[NiSO_4]^0$ included. TP207 bed, 80 °C, feed rate 8 BV/h, feed solution 0.017 M $NiSO_4$.

2. Experimental

2.1. Materials

Lewatit TP 207 (Lanxess, supplied by Sigma-Aldrich) is a macroporous poly(styrene-co-divinylbenzene) resin containing iminodiacetate (*ida*) groups. The resin was converted to acid form using 1.0 mol/L sulfuric acid and washed copiously with purified water. Properties of the resin are listed in Table 1. Highest operating temperature is according to the manufacturer 80 °C and after about 50 loading/regeneration cy-

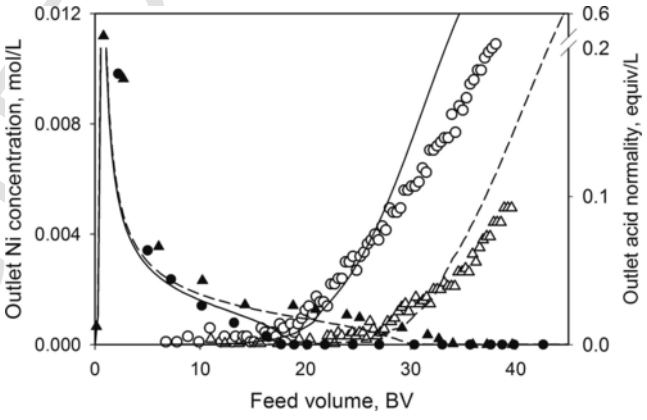

Fig. 4. Nickel (filled circles) and acid (open circles) breakthrough curves for feed solution D in TP 207. T = 22 °C (A) and 80 °C(B),

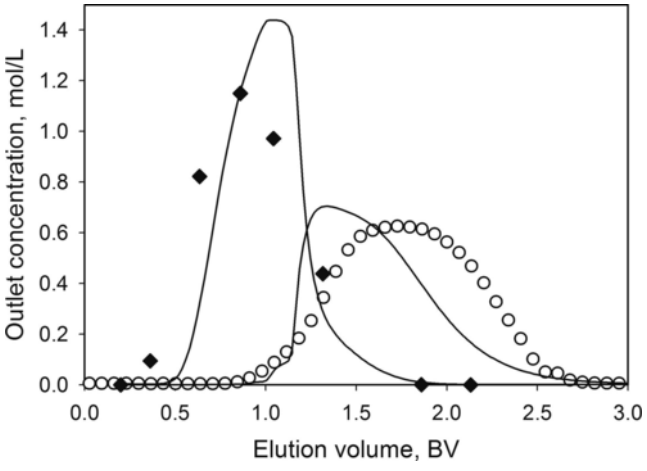

Fig. 5. Outlet concentration profiles of Ni^{2+} (circles) and NH_4^+ (diamonds) in regeneration of the TP 207 bed with 1.0 mol/L H_2SO_4 at 80 °C.

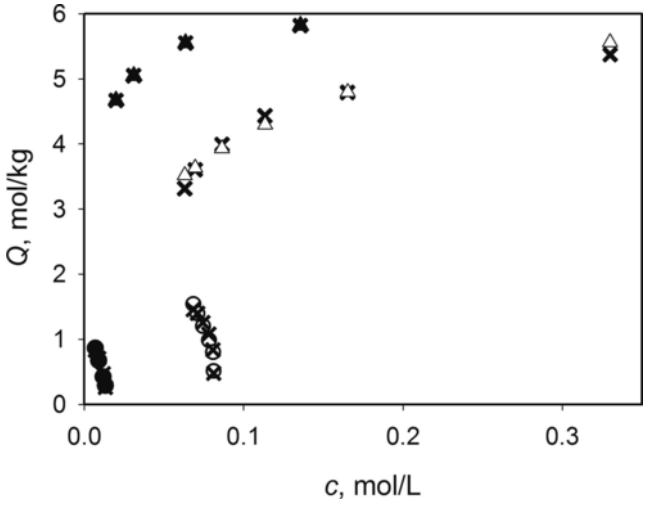

Fig. 6. Equilibrium uptake of H^+ (triangles) and Ni^{2+} (circles) at 80 °C. $c_{Ni}{}^0 = 0.01$ mol/L (filled symbols) and $c_{Ni}{}^0 = 0.10$ mol/L $NiSO_4$ solution. The crosses represent calculated values.

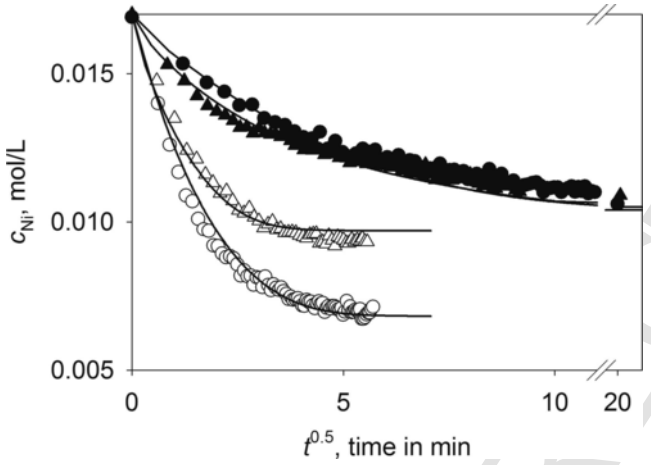

Fig. 7. Uptake kinetics for nickel in TP 207 at 22 (filled symbols) and 80 °C (open symbols). Circles and triangles refer to sulfate and chloride solutions, respectively. Continuous lines are model calculations.

cles made in this study at this temperature, no deterioration was observed.

The feed solutions given in Table 2 were prepared using reagent grade chemicals obtained from Sigma-Aldrich (NiSO4, 98%; $(NH_4)_2SO_4$, 98%; H_2SO_4, 98%; NH_4OH, 25%). Ultrapure water was used in all experiments (Centra R 60/120, >15 MΩ).

2.2. Methods

Resin density ρ_s means here the solid content in the dry resin and it was measured by drying a given volume of the water-swollen resin at 90 °C. Resin porosity was measured by adding pure water in dried resin stirred gently with a magnetic bar. The point of incipient wetness was attained, when all free-flowing particles became sticky but no free water was visible. The average particle size was obtained using laser diffraction measurements (Mastersizer 3000, Malvern). The bed capacity was measured by frontal $NH_4{}^+/H^+$ exchange at 22 °C using 0.58 mol/L NH_4OH and 0.50 mol/L H_2SO_4.

Exchange kinetics was measured in a closed glass vessel equipped with a stirrer and a recirculation pump for on-line UV–vis measurements. The stirring rate was 1000 min^{-1}. A flow-through quartz cuvette was used and the spectra were recorded at specified intervals with Cary 8454 (Agilent) spectrometer. The nickel concentration was calculated with an extinction coefficient 5.32 L/(mol cm) determined at 395 nm and using 500 nm as reference wavelength. After adjustment of the initial nickel concentration and temperature, a known amount of H-form resin was added. Nickel concentration was monitored with the on-line measurements and after the equilibrium was attained, a known volume of 4 mol/L H_2SO_4 was injected to desorb part of nickel. When the equilibrium was again established, a new portion of sulfuric acid was added. At the end of the experiment with solution D, the loaded resin was packed in a column and regenerated 1.0 mol/L H_2SO_4. The collected solution was analyzed for $NH_4{}^+$ and Ni^{2+}.

In fixed-bed experiments, the resin was packed in a jacketed glass column (ID 15 mm) and the bed volume (BV) was 22 or 106 mL. The column was attached to a precision pump (Knauer) and the outlet stream was analyzed on-line for conductivity and UV absorption at 365–395 nm. Absorbance at 500 nm was used for baseline correction. Bed temperature was controlled by thermostated water circulated in the column jacket. In feed D (Table 2), solution pH was adjusted to 7.1–7.8 by means of 25 wt% aqueous ammonia. After the loading step, the resin was washed with water and then 1.0 mol/L H_2SO_4 was pumped through the bed until all nickel was eluted.

Samples taken in stirred-tank and fixed-bed experiments were analyzed using off-line UV–vis spectroscopy (Cary 8454, Agilent) and ICP-OES (iCAP Duo 7600, Thermo Fisher Scientific) for nickel, and pH measurements and/or potentiometric titration (T50, Mettler Toledo) for the acid. Ammonium ion was analyzed using a C/N analyzer (TNM-L, Shimadzu).

3. Theory

3.1. Equilibrium model

Ion exchange in a $NiSO_4$-$(NH_4)_2SO_4$-NH_3/resin system involves several exchange and adsorption equilibria as shown in Eq. (1). R-*ida*H_2 stands for the iminodiacetic acid resin.

Table 3
Model parameters for the studied systems at 22 and 80 °C.

Anion	T, °C	*h*, –			log*κ*, –		ARD, %[a]	D_p, 10^{-10} m^2/s	
		H	Ni	Na/NH_4	Ni	Na/NH_4		H	Ni
$SO_4{}^{2-}$	22	1.000	0.8637	–	1.278	–	8.6 (8)	1.5	0.60
	80	1.000	0.8258	1.0000	−0.8151	−4.5000	4.2 (20)	10	5.0
Cl^-	22	1.000	0.8403	–	−1.5152	–	7.3 (8)	2.0	0.80
	80	1.000	0.8837	–	−1.075	–	6.8 (22)	15	7.0

[a] Number of data points in parentheses.

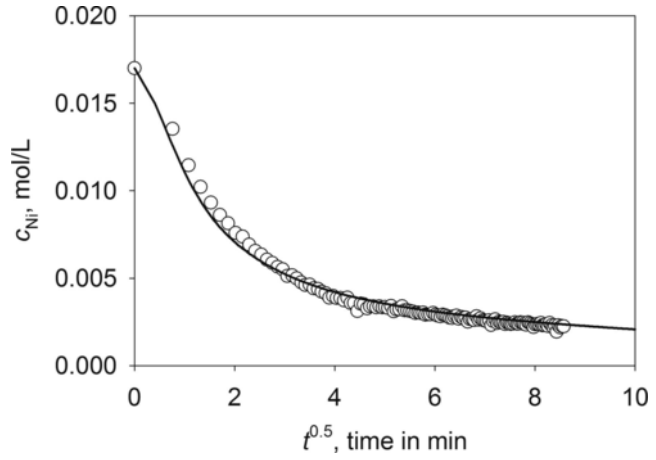

Fig. 8. Nickel uptake kinetics from feed solution D in TP 207 at 80 °C. Initial pH was 7.7. Continuous line represents model calculations.

$$R - ida H_2 + Ni^{2+} \rightleftarrows R - ida Ni + 2H^+ \quad (1a)$$

$$R - ida H_2 + NH_4^+ \rightleftarrows R - ida HNH_4 + H^+ \quad (1b)$$

$$R - ida H_2 + NH_3 \rightleftarrows R - ida HNH_4 \quad (1c)$$

Ion exchange equilibria were described using the explicit model derived earlier [13] from the NICA adsorption model of Kinniburgh et al. [14]. Consequently, the uptake of a given counter-ion is given by Eq. (2a) [13], where z_R and q_{max} are the valence and total amount of the functional groups, κ is the affinity coefficient and h is a parameter related to binding stoichiometry. Concentration in the resin pores is represented by c_p and at equilibrium it equals the bulk concentration c. Ammonia adsorption on protonated sites (Eq. (1c)) was described by Langmuir equation (Eq. (2b)) and $K_{NH3} = 500$ L/mol was used to ensure practically irreversible adsorption.

$$q_i = \frac{|z_R| q_{max} h_i (\kappa_i c_{p,i})^{h_i}}{\sum_{j=1}^{N} |z_j| h_j (\kappa_j c_{p,j})^{h_j}} \quad (2a)$$

$$q_{NH_3} = \frac{q_H K_{NH_3} c_{p,NH_3}}{1 + K_{NH_3} c_{p,NH_3}} \quad (2b)$$

In Eq. (2), q means the concentration in the solid polymer and the total uptake is given by $Q_i = \varepsilon_p c_{p,i} + (1 - \varepsilon_p) q_i$, where ε_p is the resin porosity. For simplicity, κ_H and h_H in Eq. (2a) were put equal to unity and the affinities of other ions are thus given with respect of H^+.

The concentrations in Eq. (2a) refer to cations and in the studied systems they are not necessarily equal to the stoichiometric concentrations because of number of complexation and dissociation reactions taking place in solution (Eqs (3a)–(3d)). Using the equilibrium constants discussed below in Section 3.4 and the mass balances, concentrations of all species were calculated and the values of free cations were then used in Eq. (2a).

$$Ni^{2+} + SO_4^{2-} \rightleftarrows [NiSO_4]^0 \quad (3a)$$

$$HSO_4^- \rightleftarrows H^+ + SO_4^{2-} \quad (3b)$$

$$NH_4^+ \rightleftarrows NH_3 + H^+ \quad (3c)$$

$$Ni^{2+} + nNH_3 \rightleftarrows [Ni(NH_3)_n]^{2+} \quad (3d)$$

3.2. Mass transport in the resin

The accumulation rate in the solid particles was evaluated using the linear driving force (LDF) approximation of Nernst-Planck equation reported by Melis et al. [15]. However, the LDF model with constant mass transfer coefficient k_s poorly represents the uptake rate at low loadings and therefore the formulation of Yao and Tien [16] for k_s was adopted. Moreover, we assume that mass transport in the particles is controlled by pore diffusion and external film resistance was neglected. Consequently, the accumulation rate is given by Eq. (4), where d_s is the average diameter of the spherical resin particles. The overbar indicates volume-averaged values. The term on the right-hand side of Eq. (4)

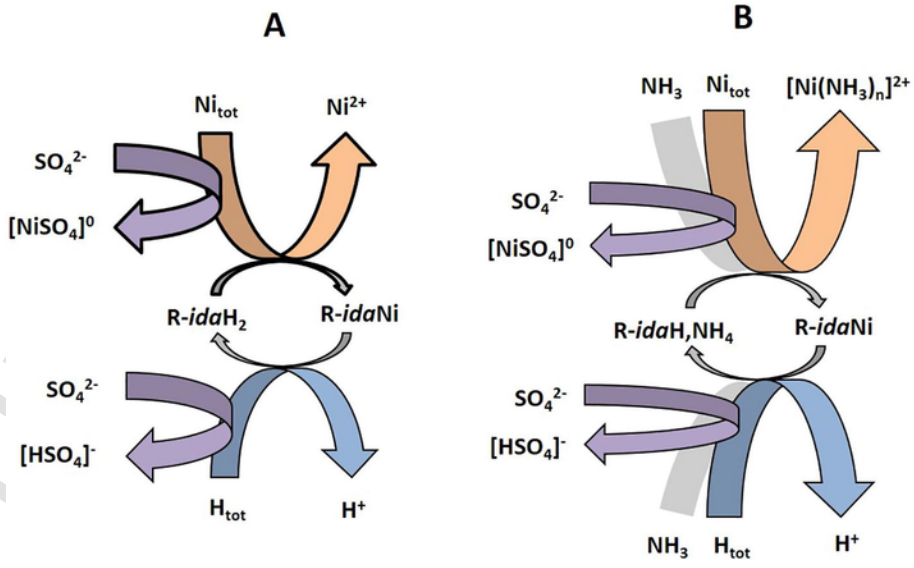

Fig. 9. Complexation by sulfate (A) and sulfate and ammonia (B) in nickel exchange on iminodiacetate groups (R-*ida*). Ni_{tot} and H_{tot} indicate the total amount of nickel and protons in the system.

refers to the speciation reactions listed in Eq. (3) and N_R is the number of reactions. Symbols ν and r stand for the stoichiometric coefficient and reaction rate.

$$\frac{d\bar{Q}_i}{dt} \approx \frac{6k_{s,i}}{d_s}\left[(c^*_{p,i}-\bar{c}_{p,i}) - z_i c^*_{p,i}\frac{\sum_j D_{p,j}(c^*_{p,ji}-\bar{c}_{p,i})}{\sum_j z_j D_{p,j} c^*_{p,i}}\right] + \varepsilon_p \sum_{j=1}^{N_R} \nu_{i,j}\bar{r}_j$$
$$k_{s,i} = \frac{4D_{p,i}}{d_s}\left(\frac{c^*_{p,i}}{\bar{c}_{p,i}} + \frac{1}{2} + \frac{\bar{c}_{p,i}}{c^*_{p,i}}\right) \quad (4)$$

Assuming that no exclusion effects are present, the concentration at the pore entrance $c^*_{p,i}$ equals the external concentration c_i. We also assume that the equilibrium conditions given in Eq. (2) are valid for the volume-averaged quantities $\bar{c}_p$ and $\bar{Q}$.

The reaction rate is written in a conventional way and as an example, Eq. (5) was used for nickel complexation with the sulfate anion (Eq. (3a)). Here c^0 is unit concentration and β is the stability constant of the $[NiSO_4]^0$ complex. The rate constant k was adjusted high enough to ensure reaction equilibrium at all calculation points. Same expression was applied to obtain the bulk reaction rate r_{NiSO4} by replacing pore concentrations with bulk concentrations. The reaction order of all components in all reactions was assumed equal to unity.

$$\bar{r}_{NiSO_4} = k_{NiSO_4}\left[\left(\frac{\bar{c}_{p,Ni}}{c^0}\right)\left(\frac{\bar{c}}{c^0}\right) - \frac{1}{\beta_{NiSO_4}}\left(\frac{\bar{c}_{p,NiSO_4}}{c^0}\right)\right] \quad (5)$$

3.3. Stirred-tank and fixed-bed models

The overall mass balance for a batch system is given by Eq. (6) assuming that the resin and liquid volumes V_S and V_L remain constant. We also assume here that the complexation reactions proceed similarly in bulk and pore solutions.

$$\frac{dc_i}{dt} + \left(\frac{V_s}{V_L}\right)\frac{d\bar{Q}_i}{dt} = \sum_{j=1}^{N_R}\nu_{i,j}r_j + \left(\frac{V_s}{V_L}\right)\varepsilon_p\sum_{j=1}^{N_R}\nu_{i,j}\bar{r}_j \quad (6)$$

Axial concentration profiles in a fixed-bed column were calculated using a discrete model described in detail elsewhere [13,17]. In this approach, the partial differential mass balance equation is replaced by the ordinary differential equation given in Eq. (7). Here, v is interstitial flow velocity, t is time, ε_b is bed porosity and ρ_s is resin density. N is the number of stirred tanks in series, L_b is the length of the bed and k is the index of the tank (*i.e.* axial position). At $k = 1$, the concentrations are equal to the feed concentrations.

$$\frac{dc_{i,k}}{dt} + v\frac{N(c_{i,k}-c_{i,k-1})}{L_b} + \left(\frac{1-\varepsilon_b}{\varepsilon_b}\right)\frac{d\bar{Q}_{i,k}}{dt} = \sum_{j=1}^{N_R}\nu_{i,j}r_j + \left(\frac{1-\varepsilon_b}{\varepsilon_b}\right)\varepsilon_p\sum_{j=1}^{N_R}\nu_{i,j}\bar{r}_j$$

Axial dispersion is not explicitly accounted for in Eq. (7) but the dispersion coefficient D_{ax} is approximately related to N as shown in Eq. (8) [13].

$$D_{ax} \approx \frac{vL_b}{2N} \quad (8)$$

3.4. Calculations

The differential Eqs. (4), (6) and (7) were solved using the methods described earlier [13]. The Simplex method was used in parameter estimation and sets of arithmetic equations were solved by the Newton method. The initial and boundary conditions for a column experiment involving both loading and elution steps are as shown in Eq. (9). The superscripts "eluent" and "feed" refer to the water eluent and the feed pulse, t_{feed} is the length of the feed pulse and function f represents the equilibrium condition given by Eq. (2). According to the boundary condition, concentrations in the first tank ($k = 1$) equals the concentrations of the incoming stream.

$$t = 0: \quad c_i = \bar{c}_i = c_i^{eluent}, \quad \bar{Q}_i = f\left(c^{eluent}\right),$$
$$0 < t \le t_{feed}: \quad c_i(k=1) = c_i^{feed}$$
$$t > t_{feed}: \quad c_i(k=1) = c_i^{eluent} \quad (9)$$

During the experiments, bed volume changed less than 5% and a constant value of 0.40 was used for ε_b. The axial dispersion coefficient, D_{ax}, was estimated from the correlation of Chung and Wen [18], and the value of N was adjusted accordingly. The average diameters and porosities of the resin particles are given in Table 1.

Goodness-of-fit to equilibrium and kinetics data in stirred tank was evaluated using the average relative deviation (ARD) defined in Eq. (10), where N_{dp} is the number of data points.

$$ARD = \frac{1}{N_{dp}}\sum_{j=1}^{N_{dp}}\left|\frac{q_{j,\exp}-q_{j,calc}}{q_{j,\exp}}\right| \times 100\% \quad (10)$$

Dissociation constants of NH_4^+ and HSO_4^- were taken from Bates et al. [19] and Knopf et al. [20], respectively. The pK_a or logβ_{HSO4} value of the bisulfate anion is 1.97 at 22 °C and 2.54 at 80 °C. The stability constant for the first *chloro* complex of nickel logβ_{NiCl} (80 °C) = −0.15 was estimated from logβ (25 °C) = −0.37 and ΔH_r = 8.2 kJ/mol [21]. The value is so small that complexation was considered unimportant and omitted in calculations. In sulfate solutions, on the contrary, substantial part of Ni forms a neutral $[NiSO_4]^0$ complex with a stability constant of logβ (25 °C) = 2.32 [22]. Using the reported [22] reaction enthalpy of 5.3 kJ/mol, the stability constant at 80 °C is 2.48. It is assumed here that only outer-sphere 1:1 complex is formed, although some evidence of inner-sphere complexation and formation of 1:2 complexes at high temperatures exists [23]. The cumulative stability constants for the *ammine* complexes were taken from Ref. [24]. Only values referring to 25 °C and zero ionic strength were found and no attempts were made to convert them to the conditions used here.

4. Results and discussion

Because of the system complexity, we first consider in Section 4.1 the Ni/H exchange (Eq. (1a)) and the influence of sulfate complexation reactions (Eqs (3a) and (3b)). Behavior of the whole system comprising of Eqs. (1) and (2) is described in Section 4.2.

4.1. Complexation with the sulfate anion

The influence of sulfate complexation on Ni uptake was studied in fixed-bed experiments with TP 207 and the nickel break-through curves were measured for 0.017 mol/L $NiCl_2$, 0.017 mol/L $NiSO_4$ and 0.017 M $NiSO_4$ containing also 1.0 mol/L of Na_2SO_4. Sodium rather than ammonium sulfate was used here to prevent precipitation of $(NH_4)_2Ni(SO_4)_2$. Although the solubility of the double salt in pure water is moderate [25], nickel is effectively precipitated in the presence of large excess of ammonium sulfate. $NiCl_2$ was used as a reference case, where nickel is present mostly as hydrated cation $Ni(H_2O)_6^{2+}$ due to the low stability of $[NiCl]^+$ [21].

The experimental break-through profiles measured at 22 and 80 °C are shown in Fig. 1. The data were correlated with the model described in Section 3 and the calculated results are given as continuous lines. Estimation of the model parameters will be discussed in Section 4.4.

Fig. 1A shows that nickel breakthrough took place almost immediately at 22 °C even when the feed rate was as low as 2.8 BV/h. The shape of the profiles suggests that nickel breakthrough at ambient tem-

perature is mainly controlled by slow intra-particle mass transport. At 80 °C (Fig. 1B), on the other hand, good uptake capacity was obtained because the equilibrium properties became dominant. Using the parameters discussed in Section 4.4 a relatively good correlation with the experimental breakthrough curves was obtained.

There is a small difference in the breakthrough curves measured in chloride and sulfate solutions at 22 °C but at 80 °C (Fig. 1B) the Ni uptake capacities are quite different. Nickel nitrate was also tested and it gave a breakthrough curve (not shown here) that was identical with that of $NiCl_2$. At the same nickel feed concentration of 0.017 mol/L, the chloride and nitrate matrices gave lowest nickel uptake and the highest was found for $NiSO_4$ at high sulfate concentration. As will be discussed later in Section 4.4, the difference is due to the equilibrium behavior and practically no difference was found in the nickel uptake rates. The result is surprising because formation of neutral sulfate complex in the solution phase should decrease nickel uptake in the resin phase. We also studied complexation of nickel with the soluble *ida* ligand at pH 4.0 and 80 °C but no difference was found between the sulfate and chloride solutions. This result indicates that there is no direct influence of the anion on formation of the nickel-*ida* complexes.

The explanation may be found in the behavior of the *ida* groups in the resin phase. After acid regeneration and washing, the groups are predominantly in the deprotonated form A shown in Fig. 2. The degree of protonation was confirmed by integration of the profiles of Fig. 1B to obtain the total amount of acid equivalents displaced by loaded nickel ions. In the sulfate solution, the H/Ni equivalent ratio was 0.97 and the maximum acid outlet concentration was 0.034 equiv/L as expected for stoichiometric exchange. Substantially higher ratio of 1.09 and a maximum acid outlet concentration of 0.040 equiv/L were found for the chloride solution. This suggests that part of the *ida* groups in this run was in the fully protonated form B releasing 3 protons and an anion when exchanged to form C ($n = 3$, $m = 1$ in Fig. 2). However, the non-stoichiometric proton desorption was not accounted for in the model calculations and same exchange mechanism was assumed for chloride and sulfate systems. In the presence of Na_2SO_4, the H/Ni ratio was 1.08 and, as indicated by the sharp initial peak in the acid profile in Fig. 1B, this is due to the H/Na exchange taking place in parallel with the H/Ni exchange.

Because the functional groups mostly are in forms A and C, there is little or no hindrance for anions to enter the resin matrix during the exchange process. We therefore propose an indirect mechanism, where complexation of *both* nickel *and* proton with sulfate is the point. The protons released in the exchange reaction are partly masked by formation of the bisulfate anion and as a result, the equilibrium shifts in favor of nickel binding. The same is true, of course, for nickel and depending on the complex stabilities, the net effect on nickel uptake can be weak as at 22 °C or strongly positive as at 80 °C. Moreover, the positive effect on nickel uptake becomes more pronounced as the sulfate concentration increases thus explaining qualitatively the behavior observed in 1.0 mol/L Na_2SO_4 (Fig. 1). The model parameters for Na^+ ($\log\kappa_{Na} = -4.80$, $h_{Na} = 1.00$) were found by trial-and-error fitting in the breakthrough curves and the same values were also used for NH_4^+ in the next Section.

In summary, the positive influence of sulfate anion on nickel exchange can be explained by complexation of the competing ion. This effect is further illustrated in Fig. 3, where the dashed line was calculated with the same model parameters as in Fig. 1 but omitting the solution-phase reactions. For comparison, the dashed line represents situation where only nickel is complexed by sulfate.

The simulated effect is qualitatively similar to that in Fig. 1 but the difference between the curves is markedly smaller than observed between the $NiCl_2$ and $NiSO_4$ curves. It is possible that the influence of bisulfate formation is further enhanced by Donnan exclusion that is not incorporated in the present model. If the negative charge of the unprotonated groups is not fully masked by the nickel cations, the bisulfate anions are expelled from the vicinity of the sites by electrostatic repulsion.

4.2. Complexation with NH_3

In the $NiSO_4$-$(NH_4)_2SO_4$-NH_3 system, nickel is effectively complexed with sulfate because of the very high SO_4^{2-}/Ni^{2+} mole ratio. However, this reaction is competed by complexation with ammonia according to the stepwise scheme of Eq. (3d). In the absence of ammonia, nickel precipitates as $(NH_4)_2Ni(SO_4)_2$ double salt, but at neutral or slightly basic ammoniacal solutions it is stabilized as *ammine* complexes. The extent of complexation depends on the concentration of ammonia and therefore Eq. (3c) also is important. In the pH range 7.0–7.7 used in this study, only lower *ammine* complexes with coordination numbers of 1 and 2 co-exist with the Ni^{2+} and $[NiSO_4]^0$. Therefore, we assume for simplicity that only $[Ni(NH_3)_2]^{2+}$ is present and the stability constant $\beta_{[Ni(NH3)2]} = 4.0$ [24] was used.

Because of the key role of ammonia, nickel breakthrough depends markedly on feed pH as shown in Fig. 4. In this case, complexation in the solution phase is much stronger than in the sulfate case but, on the other hand, the complexes still carry a positive charge and can be bound on the resin as a mixed complex or by releasing the ammine ligands. Bilewicz and Narbutt [7] have shown that decrease in the uptake of metal *ammine* complexes can be explained by partial exchange of the ammine ligands by the *ida* groups. However, they used Zn^{2+} and ammonia concentrations exceeding 1 mol/L and it is not known, whether this result can be extrapolated to concentrations used here. Therefore, a simpler approach was adopted here and the affinity coefficient κ of the $[Ni(NH_3)_2]^{2+}$ cation was adjusted by trial-and-error fitting in the breakthrough curves. The value $\log\kappa_{[Ni(NH3)2]} = -3.80$ ($h_{[Ni(NH3)2]} = 0.8258$) is much smaller than the value estimated for Ni^{2+} and it may also include contributions from steric effects and ligand exchange. Another problem in the $NiSO_4$-NH_3 system was the high ionic strength and its influence on the stability constants. The values used in Section 4.1 gave poor correlation and because no data from literature were found, following set of parameters was found by trial-and-error; $\log\beta_{[NiSO4]} = 1.00$, $\log\beta_{[HSO4]} = 1.50$, $\log\beta_{[NH4]} = 8.60$. Detailed thermodynamic studies on $(NH_4)_2SO_4$-H_2SO_4 systems have been reported [26] but considering the complexity of the present system, such rigorous treatment was not attempted.

When operating near pH 7, a good dynamic capacity was obtained even at a feed rate of 8.3 BV/h. If we assume a purification process, where the target nickel concentration in the treated ammonium sulfate solution is 10 mg/L, about 30 bed volumes can be treated in one loading/regeneration cycle. As will be shown in the next Section, the regeneration step is much shorter than the loading step and therefore high throughput rate is possible even in a simple batch-wise fixed-bed operation.

It is well-known that higher metal uptake is obtained if the *ida* groups are pre-neutralized. Therefore, one experiment was made with TP 207 pre-treated with a 3.4 mol/L $(NH_4)_2SO_4$-NH_3 solution at pH 9.0. Quite interestingly, practically no effect on the nickel breakthrough was observed although the outlet pH remained near 7 throughout the run. This result can be explained by inspecting the position of the nickel and acid fronts in Fig. 4. At pH 7.7, the nickel breakthrough point coincides with the breakthrough of ammonia and therefore the nickel front moves under nearly neutral conditions. Breakthrough of nickel and ammonia at pH 7.1 is less well-defined but again the nickel front mostly moves apart from the acidic zone. Position of the nickel front is thus mainly determined by the ammonia breakthrough, which depend on the concentration of free NH_3. In fact, the only difference in the calculated curves in Fig. 4 was the total NH_3 concentration; it was 0.036 mol/L at pH 7.1 and 0.076 mol/L at pH 7.7. The overall agree-

ment between the calculated and experimental values is not very good but the influence of feed pH on the nickel breakthrough is well explained by the model.

4.3. Regeneration of the Ni-loaded resin

After the loading step shown in Fig. 4, the resin can be easily returned back to the acid form by treatment with 1.0 mol/L H_2SO_4. Typical concentration profiles in the regeneration step are shown in Fig. 5.

Integration of the experimental outlet profiles in Fig. 5 gives the following counter-ion composition of the resin at the end of the loading step; on the equivalent basis, nickel occupies about 60% of the sites, ammonium about 30% and the rest of the groups is in the acid form. The simulated curves shown as continuous lines in Fig. 5 agree only qualitatively with the experimental profiles and the amount of NH_4^+ was somewhat overestimated. The poor agreement is probably due to uncertainty in the model parameters under such greatly varying conditions. As discussed in Section 4.4, the equilibrium parameters were estimated from data that covered acid concentrations to about 0.1 mol/L and nickel concentrations to about 0.02 mol/L. During the regeneration step, both concentrations were substantially higher and because of non-linear equilibrium condition (Eq. (2)), the calculated values are somewhat uncertain.

Preliminary tests with authentic process solutions containing also other impurity metals showed that the similar regeneration procedure is sufficient also there. The only exception is Fe^{3+} that binds on the *ida* resin much stronger than Ni^{2+} but even iron can be fully removed using higher acid concentration of 2.0 mol/L.

4.4. Determination of model parameters

The equilibrium and diffusion parameters were determined from the kinetic measurements using $NiSO_4$, $NiCl_2$ and $NiSO_4$-$(NH_4)_2SO_4$ solutions and an initial nickel concentration of 0.017 mol/L. As an example, the equilibrium data measured at 80 °C for the sulfate solution and nickel uptake curves of $NiCl_2$ and $NiSO_4$ at 22 and 80 °C are shown in Figs. 6 and 7. The best-fit values are given as continuous lines or as crosses. The estimated parameter values for all systems are listed in Table 3. As discussed in Section 3.1, the equilibrium parameters were fixed for H^+ and the κ and h values of Ni^{2+} were determined. Goodness of the fit was characterized by the ARD value calculated from Eq. (9). The pore diffusion coefficients D_p were estimated by trial-and-error from the data of Fig. 7.

The uptake curves of Fig. 7 clearly demonstrate the effect of temperature on the exchange rate. At 80 °C, the equilibrium was attained in about 20 min, while at ambient temperature several hours were needed. In terms of pore diffusion coefficients given in Table 3, the difference is nearly one order of magnitude and it is sufficient to bring about the large difference in the position and shape of the breakthrough curves of Fig. 1.

The influence of the anion was seen only in the equilibrium nickel uptake at 80 °C, while the diffusion rates in sulfate and chloride solutions were identical at 22 °C within the experimental accuracy. According to Fig. 7, the nickel uptake from sulfate solution at 80 °C was nearly twice as high as at 22 °C, while the difference in chloride solution was much smaller. At ambient temperature the anion had practically no effect on nickel uptake in agreement with the results of Littlejohn and Vaughan [5]. They measured nickel uptake in TP 207 from sulfate and mixed sulfate/chloride solutions at 25 °C and found no significant difference.

In the ammoniacal ammonium sulfate solution, model parameters for the *ammine* complex were also needed. This value together with the speciation reaction parameters were estimated in Section 4.2 from the breakthrough data. These values and the diffusion coefficients of Table 3 gave relatively good agreement with the batch uptake data measured at 80 °C using the feed solution D at pH 7.7 (Fig. 8). For simplicity, the diffusion coefficient of nickel was used for all species except H^+. The stoichiometric NH_3 concentration at $t = 0$ was 0.076 mol/L. In the end of the experiment, the resin contained 0.48 and 0.92 equiv/L of NH_4^+ and Ni^{2+}. The simulated values were 0.47 equiv/L for ammonium and 0.91 equiv/L for total nickel.

The parameters obtained in this Section were used in simulation of the break-through curves shown in Figs. 1, 3, 4 and 5. The agreement between the calculated and experimental values is in most cases satisfactory thus corroborating the validity of the parameters.

5. Conclusions

In this paper, we have shown that complexation reactions taking place in bulk and pore solution significantly affect metal binding in a chelating ion exchanger. Even weak outer-sphere interactions with the sulfate anion give rise to a surprisingly large effect on nickel breakthrough in an iminodiacetate (*ida*) resin. The unexpectedly large nickel uptake observed in sulfate solution at 80 °C is explained by enhanced complexation of the competing ion H^+ as bisulfate anion. As shown schematically in Fig. 9A, masking of both Ni^{2+} and H^+ take place and at elevated temperatures, the balance becomes favorable for nickel uptake. Such indirect mechanism may be useful in other ion exchange or adsorption systems, too.

Formation of *ammine* complexes in the $NiSO_4$-$(NH_4)_2SO_4$-NH_3 system stabilizes nickel against precipitation at pH values around 7 and high nickel loading is achieved because no competition by H^+ is present. Competition by NH_4^+ is much weaker and high Ni uptake is possible even at high ammonium sulfate concentrations. In this case, too, complexation affects indirectly by minimizing the influence of competing processes and the system is illustrated in Fig. 9B. As a result, nickel can be removed effectively even at high throughput rates provided, that elevated temperatures are used to overcome mass transport limitations. In this study, exchange with H^+, Na^+ and NH_4^+ was considered but the same approach can easily be extended to systems, where more competing cations are present. For example, selectivity of the *ida* resin for alkaline earth metals is relatively low and they do not interfere with nickel recovery. On the other hand, Fe^{3+} and other three-valent metals bind very strongly and special methods, such as step-wise regeneration, are needed to separate them from nickel.

Funding

This work was supported by Business Finland and CMEco project partners (Norilsk Nickel Harjavalta Oy, Boliden Harvalta Oy, Boliden Kokkola Oy, Outotec (Finland) Oy, Fortum Waste Solutions Oy, and Outokumpu Stainless Oy).

Declaration of Competing Interest

None.

Acknowledgement

The authors thank Mr. Tommi Huhtanen for assistance in experimental and analytical work.

References

[1] Ion Exchangers, K. Dorfner (Ed.), de Gryuter, Berlin, 1991.
[2] M. Streat, D. Naden (Eds.), Critical Reports on Applied Chemistry, vol. 19, John Wiley & Sons, Chichester, 1987.
[3] K.C. Sole, M.B. Mooiman, E. Hardwick, Ion exchange in hydrometallurgical processing: an overview and selected applications, Sep. Purif. Rev. 47 (2018) 159–178.

[4] P.E. Franco, M.T. Veit, C.E. Borba, G. da Cunha Gonçalves, M.R. Fagundes-Klen, R. Bergamasco, E.A. da Silva, P.Y. Ramos Suzaki, Nickel(II) and zinc(II) removal using Amberlite IR-120 resin: ion exchange equilibrium and kinetics, Chem. Eng. J. 221 (2013) 426–435.
[5] P. Littlejohn, J. Vaughan, Selectivity of commercial and novel mixed functionality cation exchange resins in mildly acidic sulfate and mixed sulfate–chloride solution, Hydrometallurgy 121–124 (2012) 90–99.
[6] A. Ma, A. Abushaikha, S.J. Allen, G. McKay, Ion exchange homogeneous surface diffusion modelling by binary site resin for the removal of nickel ions from wastewater in fixed beds, Chem. Eng. J. 358 (2019) 1–10.
[7] A. Bilewicz, J. Narbutt, Specific and nonspecific interactions of ammine complexes of silver, zinc, and cadmium with ion exchangers, Solvent Extr. Ion Exchange 13 (1995) 1083–1095.
[8] Z. Samczynski, R. Dybczynski, Ion exchange behaviour of cadmium on amphoteric ion exchange resin retardion lIAS and its application for the determination of cadmium in biological materials by neutron activation analysis, Chem. Anal. (Warsaw) 41 (1996) 873–890.
[9] Y. Marcus, A.S. Kertes, Ion Exchange and Solvent Extraction of Metal Complexes, Wiley-Interscience, London, 1969, Ch. 5.
[10] S. Roshdi, Chemical Modeling of Ammoniacal Solutions in Ni/Co Hydrometallurgy, University of Toronto, Thesis, 2011, Available at: https://tspace.library.utoronto.ca/bitstream/1807/31412/1/Roshdi_Sam_201111_MASC_Thesis.pdf.
[11] P. Pajunen, M. Sheedy, Metal Removal and Recovery from Process Solutions Using Short Bed Ion Exchange, Eco-Tec Technical paper 181. Available at: http://www.eco-tec.com/pdf/TP%20181.pdf (last accessed 5.11.2018).
[12] M. Sheedy, Recoflo® Ion Exchange Technology, Proc. TMS Annual Meeting, San Antonio, Texas, 1998. Available at: http://www.eco-tec.com/pdf/TP137.pdf (last accessed 15.10.2018).
[13] M. Laatikainen, M. Sillanpää, T. Sainio, Comparison of process configurations for arsenic removal with ion exchange, Desalin. Water Treat. 57 (2016) 13770–13781.
[14] D.G. Kinniburgh, H. van Riemsdijk, L.K. Koopal, M. Borkovec, M.F. Benedetti, M.J. Avena, Ion binding to natural organic matter: competition, heterogeneity, stoichiometry and thermodynamic consistency, Colloids Surfaces A 151 (1999) 147–166.
[15] S. Melis, J. Markos, G. Cao, M. Morbidelli, Ion-exchange equilibria of amino acids on a strong acid resin, Ind. Eng. Chem. Res. 35 (1996) 1912–1920.
[16] C. Yao, C. Tien, Approximations of uptake rate of spherical adsorbent pellets and their application to batch adsorption calculations, Chem. Eng. Sci. 48 (1993) 187–198.
[17] M. Laatikainen, K. Laatikainen, J. Heinonen, T. Sainio, Recovery of metal oxoanions from basic solutions using cooperative sorption – separation of Na_2MoO_4 and NaOH, Chem. Eng. J. 341 (2018) 578–587.
[18] S.F. Chung, C.Y. Wen, Longitudinal dispersion of liquid flowing through fixed and fluidized beds, AIChE J. 14 (1968) 857–866.
[19] R.G. Bates, G.D. Pinching, Acidic dissociation constant of ammonium ion at 0 to 50 C, and the base strength of ammonia, J. Res. Nat. Bur. Standards 42 (1949) 419–430.
[20] D.A. Knopf, B.P. Luo, U.K. Krieger, T. Koop, Thermodynamic dissociation constant of the bisulfate ion from Raman and ion interaction modeling studies of aqueous sulfuric acid at low temperatures, J. Phys. Chem. A 107 (2003) 4322–4332.
[21] H. Gamsjäger, Chemical Thermodynamics of Nickel. Available at: https://www.oecd-nea.org/dbtdb/pubs/vol6-nickel.pdf (last accessed 5.6.2018).
[22] S. Katayama, Conductometric determination of ion-association constants for magnesium and nickel sulfates in aqueous solutions at various temperatures between 0 °C and 45 °C, Bull. Chem. Soc. Jpn. 46 (1973) 106–109.
[23] D.B. Bechtold, G. Liu, H.W. Dodgen, J.P. Hunt, An oxygen-17 nuclear magnetic resonance study of the Aquo nickel(II) sulfate system, J. Phys. Chem. 82 (1978) 333–337.
[24] J.A. Dean (Ed.), Lange's Handbook of Chemistry, 15th ed., MacGraw-Hill, 1999.
[25] J.W. Mullin, M.M. Osman, Diffusivity, density, viscosity and refractive index of nickel ammonium sulfate aqueous solutions, J. Chem. Eng. Data 12 (1969) 516–517.
[26] S.L. Clegg, S. Milioto, D.A. Palmer, Osmotic and activity coefficients of aqueous $(NH_4)_2SO_4$ as a function of temperature, and aqueous $(NH_4)_2SO_4$-H_2SO_4 mixtures at 298.15 K and 323.15 K, J. Chem. Eng. Data 41 (1996) 455–467.